Turning Forbidden Transitions into Dominant Transitions

Nicholas Rivera, Ido Kaminer, & Marin Soljačić

Department of Physics, MIT, Cambridge, MA 02139, USA

† *Corresponding author e-mail: nrivera@mit.edu*

arXiv:1611.04048v1 [physics.optics] 12 Nov 2016

Surface phonon polaritons are hybrid modes of photons and optical phonons that can propagate on the surface of a polar dielectric. In this work, we show that the precise combination of confinement and bandwidth offered by surface phonon polaritons allows for the ability to take forbidden transitions and turn them into the primary means by which an electron emits light. We show that high-order multipolar transitions and two-photon emission processes can be over an order of magnitude faster than competing dipole transitions, as opposed to being as much as eight to ten orders of magnitude slower in free space. Our results have direct implications for the design of fundamentally new types of emitters in the mid and far IR: ones which prefer to change their angular momentum by large amounts and also ones that prefer to emit a relatively broad spectrum of entangled photons - potentially allowing for new sources of both single and multiple photons.

INTRODUCTION

Plasmonics – an extremely active field of research for several decades – can be seen as the study of the consequences of confining electromagnetic fields to regions much smaller than the wavelength of a far-field photon at the same frequency [1]. Such confinement allows for amplification of electromagnetic fields, thus enabling enhanced Raman scattering [2, 3], the ability to enhance the inherently weak nonlinearities of materials [4], and even the potential to access light-matter interaction processes in atomic-scale emitters which for almost a century have been considered generally inaccessible and thus have been considered generally inconsequential [5–14].

In particular, plasmons have been observed in 2D conductors [15–28] which are so strongly confined over a broad spectral band that it may be possible to access all sorts of transitions that are so slow that they are effectively forbidden, such as high-order multipole transitions, two-plasmon spontaneous emission processes, and spin-flip phosphorescence processes [8]. However, with such a broadband enhancement of forbidden transitions comes a price: it becomes difficult to pick a particular forbidden transition and make it dominant over all other competing processes. This is especially challenging if one of the competing transitions is a single-photon dipole transition, which will generally be faster by at least one or two orders of magnitude.

Control over forbidden transitions represents a fundamental challenge, which to our knowledge has not been addressed, and has almost never even been considered, mainly because of how difficult it is to get forbidden transitions to happen at all, let alone be dominant processes. Never-

theless, control over forbidden transitions is a very attractive goal whose realization could allow for the systematic design of new classes of emitters. It allows one to design an emitter which prefers to decay via multipolar or spin-forbidden transitions, allowing one to tune the radiation pattern of an emitter and re-shape the radiative interactions between different emitters. Realizing this goal allows one to create emitters which prefer to emit multiple entangled photons simultaneously, rather than a single photon, which could potentially lead to new sources of single photons and also entangled photons [29]. Moreover, it could allow us to take a single emitter and use it to emit radiation with a tunable frequency and angular spectrum, when conventionally its frequency and angular spectrum is relatively fixed.

As we show here, an emerging class of photonic materials may provide a route to realize control over forbidden transitions. Polar dielectrics like hexagonal boron nitride (hBN) and silicon carbide (SiC) have been the subject of significant attention over the past two years due to their ability to confine electromagnetic energy in small volumes (on length scales potentially as short as 5 nm), just like plasmons in 2D materials [30–42]. Unlike 2D plasmons, the surface phonon-polaritons (SPhPs) of these materials only have extremely strong confinement (comparable to/higher than graphene) over a relatively narrow spectral band of a few THz. Moreover, these phonon polaritons can have substantially lower losses than plasmons [43].

In this work, we study the consequences of narrow-band strongly confined light for quantum nanophotonics. In particular, we show that phonon polaritons allow for the ability to access forbidden transitions with extremely high efficiency. We show that multipolar transitions and multiphoton emission processes can be made dominant over all other competing transitions. As a special case, we show how phonon-polaritons may allow for the design of a new kind of quantum optics source, emitting entangled pairs at rates over an order of magnitude larger than any competing one-photon transitions. Our results may allow for the possibility of ushering in new classes of quantum emitters with tunable multipolarity and/or tunable emission spectra, in addition to new materials for broad-band absorption/emission, new capabilities for IR spectroscopy, sensing platforms, and many other applications.

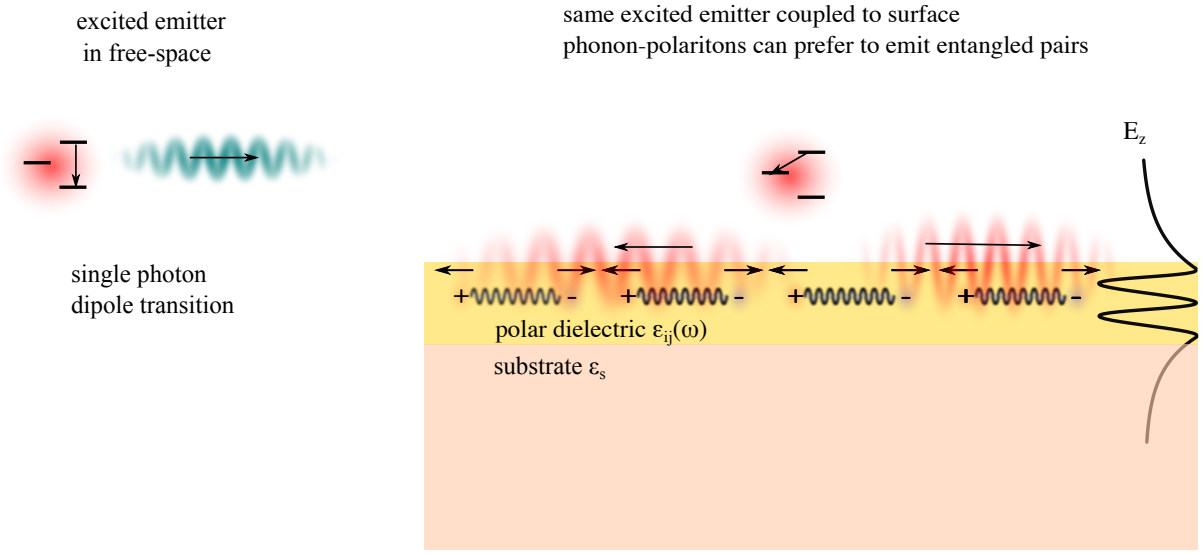

FIG. 1: **General Scheme for Accessing Forbidden Transitions at High-Efficiency:** (Left) Typical situation for an emitter (even when coupled to plasmons): an emitter may have many choices for a transition, but the relatively high-frequency single-photon dipole transition is chosen. (Right) When coupling that same excited electron to SPhPs in a polar dielectric, the electron can be made to prefer a forbidden transition in the IR (e.g; two-polariton spontaneous emission).

QUANTUM ELECTRODYNAMICS OF PHONON POLARITONS AND GENERAL SCHEME FOR HIGH-EFFICIENCY FORBIDDEN TRANSITIONS

The general scheme for accessing high-efficiency forbidden transitions is illustrated in Figure 1. In free-space (or even near highly confined 2D plasmons over a broad spectral range), an emitter given a choice between different transition pathways will generally take the single-photon E1 transition over other choices. However, if we have strongly confined modes over a narrow frequency band, then we can create a situation in which the single-photon E1 transition is negligibly enhanced while a forbidden transition is very strongly enhanced (over 10 orders of magnitude relative to the enhancement of the competing E1 transition), so much so that this once-forbidden transition is strongly preferred.

In order to translate our intuition to a quantitative theory, we develop a formalism to compute the rates of various forbidden transitions for emitters placed near films supporting SPhP modes. We compare them to the rates of nearby *non-degenerate* transitions (because in general atoms, states with different orbital angular momenta are non-degenerate). As a case in point, we men-

tion that there exist plenty of atoms where a conventionally forbidden transition exists within the Reststrahlen band (of one of the many SPhP supporting materials) but conventionally allowed transitions do not. For example, in the lithium atom, there is a quadrupolar $d \rightarrow s$ transition at 795 cm^{-1}. All other transitions fall outside of the Reststrahlen bands. Similarly, in the very same atom, there is a $d \rightarrow s$ transition at 1611 cm^{-1}, which can potentially occur via emission of a pair of SPhPs. Again, all other competing transitions fall outside of the Reststrahlen bands. Moreover, in emitters where the level structure can be designed, as in quantum wells or dots, there should be many more possibilities for engineering conventionally disallowed transitions to fall in the Reststrahlen band of some SPhP supporting material.

To capture multipolar emission and multiphoton emission in the same formalism, fully quantum calculations are necessary. The results presented in this paper take losses into account rigorously through the formalism of macroscopic QED which we use to describe SPhPs. Light-matter interaction is characterized by an interaction Hamiltonian [44]

$$H_{int} = \frac{e}{2m}(\mathbf{p}\cdot\mathbf{A} + \mathbf{A}\cdot\mathbf{p}) + \frac{e^2}{2m}\mathbf{A}^2, \tag{1}$$

where the vector potential operator, $\mathbf{A}$, in the presence of losses is given by [45]:

$$A_i(\mathbf{r}) = \sqrt{\frac{\hbar}{\pi\epsilon_0}}\int d\mathbf{r}'\int d\omega'\frac{\omega'}{c^2}\sum_{k'}\sqrt{\text{Im }\epsilon(\mathbf{r}',\omega')}\left(G_{ik'}(\mathbf{r},\mathbf{r}',\omega')\hat{f}_{k'}(\mathbf{r}',\omega') + \text{H.c}\right), \tag{2}$$

with $G_{ik'}(\mathbf{r},\mathbf{r}',\omega')$ being the dyadic Green function of the Maxwell equations for the material system presented on the right side of Figure 1. For the low losses characteristic of phonon-polaritons (and even often plasmon-polaritons), decay rates can be obtained with reasonable accuracy by neglecting the losses and writing the field operators in the form of an expansion over plane-wave phonon-polariton modes. We discuss this effective mode expansion in more detail in the Supplementary Materials. The vector potential in the lossless limit takes the form:

$$\mathbf{A} = \sum_{\mathbf{q}}\sqrt{\frac{\hbar}{2\epsilon_0\omega_q}}\left(a_{\mathbf{q}}\mathbf{F}_{\mathbf{q}} + \text{H.c}\right) \tag{3}$$

The modes $\mathbf{F}_{\mathbf{q}}$ satisfy $\nabla\times\nabla\times\mathbf{F}_{\mathbf{q}} = \epsilon(\omega)\frac{\omega^2}{c^2}\mathbf{F}_{\mathbf{q}}$ and are normalized such that $\frac{\hbar\omega}{2\epsilon_0} = \int d\mathbf{r}\ \mathbf{F}^*_{\mathbf{q}}\cdot\frac{1}{2\omega}\frac{d(\epsilon\omega^2)}{d\omega}\cdot\mathbf{F}_{\mathbf{q}}$. In the vicinity of the emitter, the SPhP modes look like (neglecting retardation): $\mathbf{F} = F_0 e^{i\mathbf{q}\cdot\boldsymbol{\rho}-qz}\hat{e}(\hat{\mathbf{q}})$, where F_0 is the field amplitude and $\hat{e}(\hat{\mathbf{q}}) = \frac{1}{\sqrt{2}}(\cos\theta, \sin\theta, i)$ in Cartesian coordinates. The normalization can be proven rigorously to be consistent with a dyadic Green function formalism, as is done in [46]. In the limit where there is no dissipation, these two expressions for the vector potential operator generate equivalent decay rates, as can be shown by writing

the Green function in the limit of no losses. We show this explicitly in the Supplementary Materials. The advantage of the Green function expression is generality and the ability to characterize the impact of losses on decay rates. The advantage of the lossless formalism is that it emphasizes the fact that the emission is into modes, and from this, we can easily extract information such as the angular spectrum of emitted phonon-polaritons, as we do in Section 4. We use both formalisms throughout this work.

In multi-photon calculations where the dipole approximation is appropriate, a much more convenient choice of interaction Hamiltonian is given by $H_{int} = -\mathbf{d}\cdot\mathbf{E}$ + self-energy. The self-energy term has no creation or annihilation operators and is thus irrelevant to our calculations. Finally, we note throughout this work we assume that these phonon-polariton supporting materials are well-described by a local model (i.e., their dielectric constant is only frequency dependent). Agreement with a local model has been seen in hBN films as thin as 1 nm, although only the long-wavelength part of the dispersion was measured [31]. Nevertheless, we will see that the effects we describe below should be feasible for thicknesses between 5 and 10 nm, where a local model should suffice.

PHONON-POLARITONS ALLOW FOR CREATING PREFERENTIALLY NON-DIPOLAR EMITTERS

We start by showing that it is possible to force an electron to have as its dominant decay mechanism a multipolar single photon transition (even for multipolarities as high as 32-pole). In this section and the next, we consider a hydrogen atom for calculational simplicity. Of course, the general principle for enabling high-efficiency access to forbidden transitions is independent of whether or not the atom in question is hydrogenic, and thus our findings apply to a wide array of atoms, molecules, and artificial atoms (quantum dots/wells/wires). Our findings should be especially well-suited towards accessing conventionally slow transitions in quantum dots, whose mesoscopic dimensions lead to significantly less polaritonic confinement being required.

In Figure 2, we compare the potential of using hyperbolic (Figures 2a-2c) and non-hyperbolic (Figures 2d-2f) phonon-polariton materials to access high-order multipolar transitions at high efficiency. In all of our calculations, the optic axis of hBN is taken along the direction that the thickness is measured (z-direction). For concreteness, we consider the series of hydrogenic transitions $7\{p,d,f,g,h\}(m=0) \rightarrow 6s$ at 12.4 μm for 4H-SiC (isotropic) and hBN (hyperbolic). These transitions are respectively E1 (dipole), E2 (quadrupole), E3 (octupole), E4 (hexadecupole), and

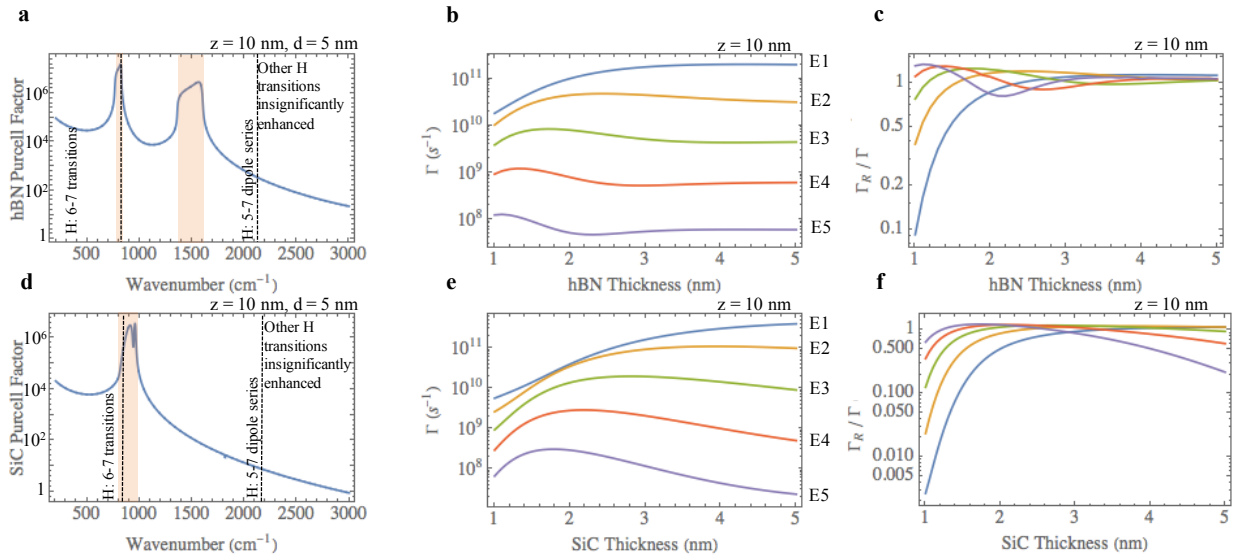

FIG. 2: **High-Efficiency Access to Multipolar Transitions:** Comparing the potential of phonon-polariton materials to force an electron to prefer decay via multipolar transitions in hBN (hyperbolic) and SiC (non-hyperbolic). (a,d) Purcell factors for a z-polarized dipole 10 nm away from hBN (a)/ SiC (d), of thickness 5 nm which is used to estimate the rates of competing dipole transitions. (b, e) Decay rates for multipolar transitions E1-E5 for an emitter 10 nm away from the surface of hBN at frequency 806.5 cm^{-1} (b) or for multipolar transitions E1-E5 for an emitter with the same multipole moments 10 nm away from the surface of SiC at frequency 920 cm^{-1} (e).(c,f) Radiative ratios Γ_R/Γ of multipolar transitions in hBN (c) and SiC (f) for the transitions considered in (b) and (e). The permittivity of the substrate is taken to be 11 for the case of hBN and 1.5 for the case of SiC. The damping constant for both materials is taken to be 5 cm^{-1}.

E5 (32-pole). In Figures 2(a) and 2(d), we plot the p-polarized Purcell spectra for a dipole emitter oriented in the z-direction (perpendicular to 5 nm thick hBN (Fig. 2a) or 5 nm thick SiC (Fig. 2d)), 10 nm above hBN/SiC in order to estimate the rates of competing dipole transitions. The Purcell spectra of course has a large peak in the Reststrahlen (RS) bands (highlighted orange in the figures), but is nonzero outside of the RS bands mostly due to losses. For both hBN and SiC, the fastest nondegenerate transition (for reasons discussed above) in competition with a 7-6 transition is the 7-5 E1 transition with a lifetime of roughly 1 μs, which has been enhanced roughly an order of magnitude by losses.

In Figure 2(b), we plot the transition rates of E1-E5 7-6 transitions for hydrogen above hBN as a function of hBN thickness. We see that for small thicknesses of around 5 nm, even the E5 transition is faster than the 7-5 E1 transition. The 7-6 transition in hydrogen also coincides with the RS band of SiC. However, we found that at the transition frequency (around 806 cm^{-1}), for a thickness of 5 nm, that the very high-order multipolar transitions were quite slow and that these decays mostly happened as a result of the losses. This happens merely because the transition frequency is too close to the lower edge of the SiC RS band, meaning that the confinement of the mode at that frequency is not very high. If we instead consider a hypothetical emitter with a transition frequency of 920 cm^{-1} but with the exact same multipole moments as those associated with the aforementioned Hydrogenic 7-6 transitions, the rates of high-order multipole transitions become extremely high (see Figure 2(e)).

It is important to have some measure of what part of the decay comes from coupling to propagating modes. Even though phonon-polaritons have relatively low loss, the effects of losses can be amplified by bringing an emitter sufficiently close to a surface which is dissipative. To this end, we define a quantity we call the radiative ratio, $r \equiv \Gamma_R/\Gamma$, which we define as the ratio of the decay rate computed assuming no losses (Γ_R) to the decay rate computed with losses taken into account (Γ). It is a measure of the extent to which quenching dominates the decay dynamics insofar as a low r value suggests strong loss-dominated decay. However, this measure is an imperfect one because it can be larger than 1, and this is simply because the effect of losses is not purely to add new decay channels. It can modify (namely reduce) the density of states of radiative channels, as is well known in the conventional Purcell effect with optical resonators.

In Figures 2c and 2f, we consider the r-values of the multipolar decays considered in Figures 2(b) and 2(e) for hBN (Figure 2c) and SiC (Figure 2f) as a function of hBN and SiC thicknesses ranging from 1 to 5 nm. We can see that there exist regimes where the radiative ratio is around 1 for the different multipolar transitions, although the behavior at larger thicknesses for hyperbolic hBN versus isotropic SiC is noticeably different. For hBN, the radiative ratio stabilizes to about 1 while for SiC, the efficiency drops more and more as the multipolar order increases. What accounts for this difference between hBN and SiC? Hyperbolicity. The decay rate of an En transition is proportional to $\int dq\, q^{2n} e^{-2qz_0}$ Im $r_p(q,\omega)$ where $r_p(q,\omega)$ is the p-polarized reflectivity of the air-polar dielectric-substrate system at the transition frequency, q is a wavevector, z_0 is the emitter-surface separation, and n is the multipolar order of the pure multipole emitter ($n = 1$ for dipole, $n = 2$ for quadrupole, etc.) This integral splits up into two parts – a pole contribution centered

at the value of q satisfying the dispersion relation, and a broad background which peaks around $\frac{1}{z_0}$. This broad background vanishes in the absence of dissipation and can often be qualitatively understood as the part of the decay rate coming from losses. Losses dominate when $\frac{1}{z_0} \gg q$. In hyperbolic systems like hBN, high-order modes can exist at q near $\frac{1}{z_0}$, meaning that losses do not dominate. On the other hand, in non-hyperbolic systems with thickness on the order of $\frac{1}{z_0}$, there are no modes there generally, and losses will dominate. This effect is especially pronounced for higher order multipole transitions because their rates depend much more sharply on wavevector.

PHONON-POLARITONS ALLOW FOR CREATING EMITTERS WHICH PREFERENTIALLY EMIT ENTANGLED PAIRS OF PHOTONS WITH A TUNABLE FREQUENCY AND ANGULAR SPECTRUM

In this section, we show that it is possible to force an electron to have two-photon spontaneous emission as its dominant transition - leading to a natural source of entangled photons. Moreover, we show that this preferential emitter of entangled photons has a tunable angular and frequency spectrum. These spectra can be tuned through knobs such as atom-surface separation, substrate index, emitter frequency. Moreover, these spectra depend heavily on the detailed electronic structure of the orbitals participating in the transition, allowing for a new degree of freedom by which to control two-polariton emitters. Heuristically, a preferential emission of entangled photon pairs will happen when there is no SPhP mode at the frequency of competing one-photon transitions, while there are SPhP modes at roughly half of the frequency of the transition in question. This is why extreme confinement ($\frac{\lambda_0}{\lambda_{SPhP}} > 100$) over a narrow band is necessary. [51] We note that for mesocopic emitters and solid-state emitters, much less enhancement is needed because the free-space rates of two-photon emission can be much larger for these systems, since two-photon emission rates scale as four powers of the characteristic emitter length [13].

We consider an electron which is put into the hydrogen 5s state and we consider the rate of decay into the 4s state by two-polariton spontaneous emission into cBN (cubic boron nitride) phonon polaritons. The frequency of the transition is 2468 cm^{-1} while the RS band of cBN is between 1052 and 1303 cm^{-1}. In Figure 3a, we compute the Purcell-spectra for a first-order dipole transition for atom-surface separations of 5, 10, and 25 nm to get an order of magnitude estimate for the rates of the competing dipole transitions at first order. At 5 nm, the fastest competing transition occurs with a lifetime of order 100 ns. At 10 and 25 nm, the order of magnitude of

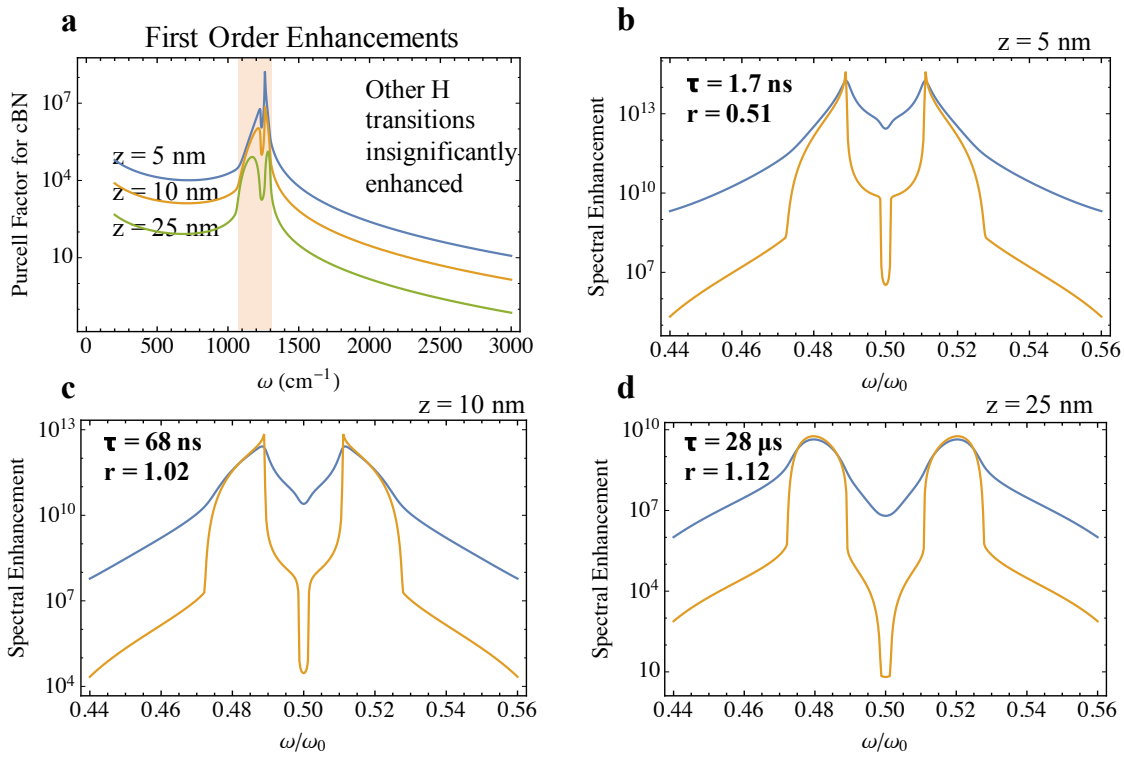

FIG. 3: **Making Two-Photon Emission Dominant:** (a) Purcell spectra for a z-polarized dipole above 10 nm thick cBN at atom-surface separations of 5, 10, and 25 nm. (b, c, d). Two-photon Purcell spectra for an s $\rightarrow$ s transition as a function of photon frequency ω for the same set of atom-surface separations. Blue denotes the Purcell spectra with losses accounted for and the orange denotes the Purcell spectra for cBN with 100x weaker losses. In each of (b,c,d) we note both the overall two-photon transition rate between the 5s and 4s states of hydrogen and the corresponding radiative ratio (Γ_R/Γ). The permittivity of the substrate is taken to be 2 and the damping constant for cBN is taken to be 5 cm^{-1}.

the competing E1 transition is closer to 1 μs. In Figures 3(b-d), we compute the spectrum of two-photon emission from 5s-4s (due to cBN phonon-polaritons), in addition to the lifetime of the two-photon transition and the r-values (as defined in the previous section).

To do this computation, we make use of a general result (that we derive in the Supplementary Materials) that for an s $\rightarrow$ s transition, the spectral enhancement factor, defined as the ratio of the SPhP emission spectra, $\frac{d\Gamma}{d\omega}$, to the free-space emission spectrum $\frac{d\Gamma_0}{d\omega}$ is given by:

$$\text{Spectral Enhancement} = \frac{\frac{d\Gamma}{d\omega}}{\frac{d\Gamma_0}{d\omega}} = \frac{1}{2}F_p(\omega)F_p(\omega_0-\omega), \tag{4}$$

where $F_p(\omega)$ is the Purcell factor for a dipole perpendicular to the surface and is related to

the imaginary part of the reflectivity of the air-polar dielectric-substrate system by $F_p(\omega) = \frac{3}{2k_0^3}\int dq\, q^2 e^{-2qz_0}\text{Im}\, r_p(q,\omega)$, where k_0 is the free-space photon wavevector, $\frac{\omega}{c}$ [47].

In Figures 3(b-d), we see that the lifetimes of two-photon spontaneous emission for an emitter 5, 10, and 25 nm away from the surface of 10 nm thick cBN are 1.7 ns, 68 ns, and 28 μs, respectively. Their r-values are 0.51, 1.02, and 1.12, respectively. Thus, two-photon spontaneous emission into phonon-polaritons can be nearly two orders of magnitude faster than single-photon dipole transitions. This is in sharp contrast to the situation in free-space, where two-photon spontaneous emission is roughly 8-10 orders of magnitude slower. We thus conclude that using phonon-polaritons, it is possible to create a source of a pair of entangled polaritons with very high efficiency. We now move on to describing the spectral properties of this new quantum light source, both in frequency and angle.

In the Supplementary Materials (Figure 5), we also considered the spectral enhancement defined above in hBN as a function of emitter frequency ($\omega_0 = 1600, 2300, 3000$ cm^{-1}) and emitter-surface separation ($z_0 = 5, 10, 15$ nm). We chose a different material than that of Figure 3 to show that two-photon spectral enhancements similar to those in thin cBN are achievable in other materials (the spectral enhancement is of the same order of magnitude as that in cBN (Figure 3)) and also to show a large number of frequency bands where a two-photon emitter can be created. What we found is that hBN offers very high spectral enhancement in three different frequency bands, as opposed to one in isotropic polar dielectrics, allowing for compatibility with many more electronic systems. The reason for this is intercombination: a two-photon emission through near-field polaritons can occur via two photons in the lower RS band, two photons in the upper RS band, or one in the upper RS band and one in the lower RS band. A material having three separate RS bands would offer six frequency ranges for two-photon emission. We also found that increasing the emitter separation causes the emission spectrum not only to be weaker, but also narrower (by about a factor of 2 when goes from 5 nm to 15 nm) . This allows one to tune not only the emission rate but also the emission spectrum with atom-surface separation.

Finally, we consider the angular spectrum of emitted photons. In the Supplementary Materials, we derive the general result that the angle and frequency spectrum of two-photon emission, $S(\omega,\theta,\theta')$ is proportional to:

$$S(\omega,\theta,\theta') \sim \left|\sum_{ij} \hat{e}_i^*(\theta)\hat{e}_j^*(\theta')T_{ij}(\omega)\right|^2, \tag{5}$$

where $T_{ij}(\omega) = T_{ji}(\omega_0-\omega) \sim \sum_n \left(\frac{d_i^{gn}d_j^{ne}}{E_e-E_n-\hbar\omega} + \frac{d_j^{gn}d_i^{ne}}{E_e-E_n-\hbar(\omega_0-\omega)}\right)$, where d^{ab} denotes a dipole

matrix element between states a and b, n denotes an intermediate atomic state, g denotes the ground state, e denotes the excited state, and E_i is the energy of the ith state. The $\hat{e}_i(\theta)$ are the phonon-polariton polarizations in the vicinity of the emitter, given by $\frac{1}{\sqrt{2}}(\cos\theta, \sin\theta, i)$

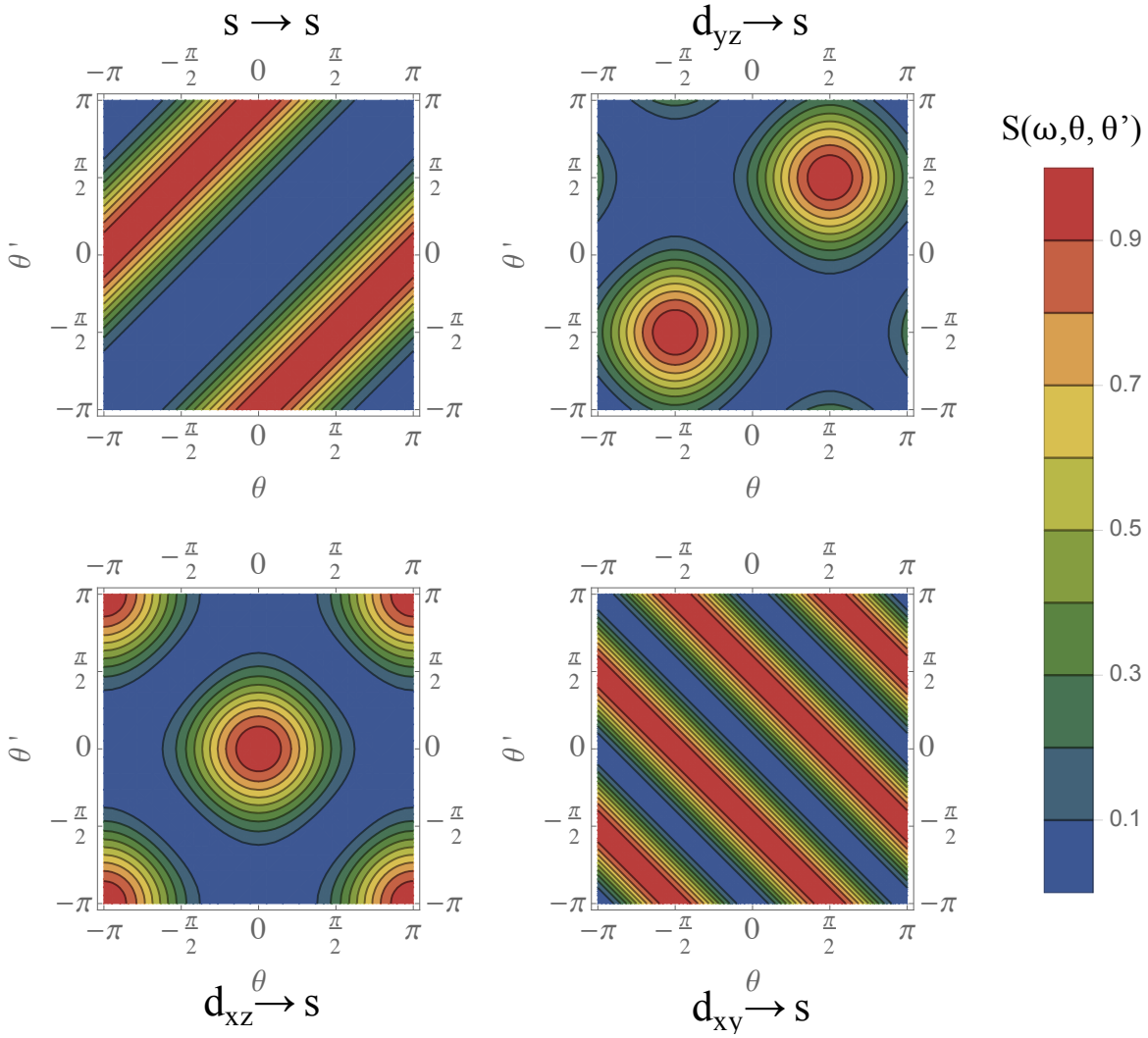

FIG. 4: **Using the Shape of the Wavefunction to Control the Angle Spectrum of Emitted Entangled Pairs:** Plots of the angular spectrum $S(\omega_0/2, \theta, \theta')$ of two-photon emission as a function of the initial state of the electron for initial states $s, d_{xy}, d_{xz}, d_{yz}$.

The angular dependence of the spectrum in Equation (5) will lead to very different angular spectra for different transitions. In Table 4.1, we show the angular spectrum as a function of different transitions (at $\omega = \omega_0/2$). Strictly speaking, the angular spectrum is frequency dependent. However, due to the narrowness of the RS band(s), this can be neglected, and thus we only consider the spectrum at half the transition frequency. Remarkably, just by changing the initial state

Transition	Angular Spectrum
$s \to s$	$\sin^4\left(\frac{\theta-\theta'}{2}\right)$
$d_{xy} \to s$	$\sin^2(\theta+\theta')$
$d_{xz} \to s$	$(\cos\theta+\cos\theta')^2$
$d_{yz} \to s$	$(\sin\theta+\sin\theta')^2$

TABLE I: A summary of the dependence of the angular spectrum of two-photon radiation as a function of initial and final electronic states for a few selected initial electronic states.

of the system, one can change whether the entangled pairs are preferentially emitted in the same direction (as in Figure 4(top right,bottom left)) or in opposite directions (as in Figure 4(top left)). The key results of this section are that: using highly confined, narrow-band phonon-polaritons, it is possible to have an electron prefer to decay via the emission of a pair of entangled photons. Moreover, it is possible to do this at many frequency ranges in the mid IR, especially in anisotropic materials such as hBN, due to their multiple Reststrahlen bands. The frequency spectrum of such a source of entangled near-field photons can be reshaped by emitter frequency and emitter-surface separation. Finally, coherent effects arising from electronic structure give us a surprisingly rich degree of freedom to tune the angular shape of the radiation. For some initial and final orbital configurations, it is possible to have the entangled pairs prefer to go in the same direction, while in others, pairs strongly prefer to travel in opposite directions. There are a number of ways to populate a particular initial state. One is by exciting the atoms with light of a fixed polarization. Another, appropriate in systems with less extreme degeneracy than hydrogen, is to simply excite the atoms with the appropriate frequency.

SUMMARY

In summary, we have shown that the unique combination of extremely high confinement factors ($\frac{\lambda_0}{\lambda_{SPhP}}$ over 200) and a narrow, but not too narrow spectral range allows for the design of atomic emitters fundamentally different than any that have been realized before. We can use phonon-polaritons to design emitters which preferentially emit via multipolar transitions, allowing us to reshape the radiation of emitters and the radiative interaction between different emitters. We found that this effect can happen both in hBN and in thin polar dielectrics, although in hBN, the emission can be enhanced for a larger range of system parameters, due to hyperbolicity. Moreover, using this

general technique of extremely high confinement over a narrow spectral range, we can also design emitters which preferentially decay via the emission of entangled pairs of near-field photons, even when single-photon dipole transitions are allowed. We found that this can be realized over many frequency ranges in the mid-IR, that the frequency spectra are relatively broad and tunable, and that coherent quantum effects can completely reshape the angular spectrum of emission of these entangled pairs. This last finding suggests the possibility to use shaped electron wave packets to reshape the spectrum of entangled photon radiation.

As all atoms have electronic transitions in the mid-IR, our results should apply to a large portion of the periodic table. It may also be possible that vibrational transitions may be used to observe these effects, although one obstacle towards realizing these effects with molecular vibrations is the generally low multipole moments associated with vibrational transitions (1 Debye dipole moments for example). Moving beyond the mid-IR to the near-IR, it may be possible to realize the effects we describe here using 'shaped polaritonic media' (such as nano-resonators of graphene or plasmonic crystals of graphene and other 2D plasmonic materials) supporting (respectively) narrow spectral response or photonic bandgaps. We believe that these results may have direct implications for: spectroscopy for inferring electronic transitions which cannot be determined with photons, sensors based on forbidden transitions, quantum radiation sources (on-demand generation of single photons and entangled pairs of photons), new platforms for quantum non-linear optics, the possibility of realizing nonlinearities at the single photon level, the ability to turn narrow-band emitters into broadband emitters, the ability to turn narrow-band absorbers into broadband absorbers, and most generally, the ability to completely reshape the ostensibly fixed optical properties of materials.

ACKNOWLEDGEMENTS

This work was partly supported by the Army Research Office through the Institute for Soldier Nanotechnologies under contract no W911NF-13-D-0001. M.S. (analysis and reading of the manuscript) was supported by S3TEC, an Energy Frontier Research Center funded by the US Department of Energy under grant no. de-sc0001299. I.K. was supported in part by Marie Curie grant no. 328853-MC-BSiCS. We also thank J. D. Joannopoulos, E. Ippen, J.J. Lopez, and B. Zhen for fruitful discussions.

SUPPLEMENTARY MATERIALS FOR: TURNING FORBIDDEN TRANSITIONS INTO DOMINANT TRANSITIONS

In this appendix, we derive some results regarding the coupling of atomic emitters to the phonon-polaritions characteristic of polar crystals such as hBN and SiC. In particular, we consider atom-field interactions governed by the non-relativistic Pauli-Schrodinger Hamiltonian H:

$$\begin{aligned} H &= H_a + H_{em} + H_{int} \\ H_a &= \left(\sum_i \frac{\mathbf{p}_i^2}{2m_e} - \frac{e^2}{4\pi\epsilon_0 r_i} \right) \\ H_{em} &= \sum_k \int d\mathbf{r} \int d\omega \, \hbar\omega \left(f_k^\dagger(\mathbf{r},\omega) f_k(\mathbf{r},\omega) + \frac{1}{2} \right) \\ H_{int} &= \sum_i \frac{e}{2m} (\mathbf{p}_i \cdot \mathbf{A}(\mathbf{r}_i) + \mathbf{A}(\mathbf{r}_i) \cdot \mathbf{p}_i) + \frac{e^2}{2m} \mathbf{A}^2(\mathbf{r}_i), \end{aligned} \tag{6}$$

H_a is the atomic Hamiltonian, H_{int} is the atom-field interaction and $\mathbf{A}$ is the vector potential operator. The minimal-coupling interaction Hamiltonian presented above is related to the more well-known dipole interaction Hamiltonian: $-\mathbf{d} \cdot \mathbf{E}$ + self-energy, by a unitary transformation in the long-wavelength (dipole) approximation [48].

The approach that we take accounts for losses via the formalism of macroscopic QED. The primary physical difference between QED without losses and QED with losses lies in the elementary excitations. In the lossless formalism, the excitations can be seen as quanta of electromagnetic modes. In the lossy formalism, the excitations cannot be seen as quanta of electromagnetic modes because the modes are no longer complete. Rather, the elementary excitations are point dipoles which are induced in the material. These excitations are characterized by position, frequency, and orientation.

The vector potential operator in the framework of macroscopic QED is given by:

$$A_i(\mathbf{r}) = \sqrt{\frac{\hbar}{\pi\epsilon_0}} \int d\omega' \, \sum_j \frac{\omega'}{c^2} \int d\mathbf{r}' \sqrt{\text{Im } \epsilon(\mathbf{r}',\omega')} G_{ij}(\mathbf{r},\mathbf{r}';\omega') \hat{f}_j(\mathbf{r}',\omega') + \text{H.c.}, \tag{7}$$

where G_{ij} is the dyadic Green function of the Maxwell equations, satisfying $\nabla \times \nabla \times \mathbf{G}_i - \epsilon(\mathbf{r},\omega)\frac{\omega^2}{c^2}\mathbf{G}_i = \delta(\mathbf{r}-\mathbf{r}')\hat{e}_i$. The operator $\hat{f}_j^{(\dagger)}(\mathbf{r},\omega)$ annihilates (creates) a lossy excitation of frequency ω, at position $\mathbf{r}$, and in direction j. It satisfies bosonic commutation relations, namely: $\left[\hat{f}_i(\mathbf{r},\omega), \hat{f}_j^\dagger(\mathbf{r}',\omega')\right] = \delta_{ij}\delta(\omega-\omega')\delta(\mathbf{r}-\mathbf{r}')$. When applying the Fermi Golden Rule, the initial state is $|e,0\rangle$, while the final states are of the form $|g,\mathbf{x}_1\omega_1 k_1, ...\mathbf{x}_N\omega_N k_N\rangle$ [45], where g represents

a ground atomic state, e represents an excited atomic state, and $|\mathbf{x}\omega k\rangle \equiv \hat{f}_k^\dagger(\mathbf{x},\omega)|0\rangle$ represents an excitation of the electromagnetic field.

Optical Response of Phonon-Polariton Materials

As prescribed by Equation (7), we must compute the Green function of a phonon-polariton supporting system. The simplest computation involves invoking the excellent approximation that the wavevector of the emitted phonon polaritons is much larger than the photon wavelength $\frac{\omega}{c}$. This is the electrostatic limit. In such a limit, the electric field is approximately longitudinal, i.e; $\mathbf{E} = -\nabla\phi$, where ϕ satisfies the Laplace equation: $\sum_{ij} \partial_i \epsilon_{ij}(\omega)\partial_j \phi = 0$. The Green function for the potential $G_\phi(\mathbf{r},\mathbf{r}',\omega)$ is defined by: $\sum_{ij} \partial_i \epsilon_{ij}(\omega)\partial_j G_\phi(\mathbf{r},\mathbf{r}',\omega) = \delta(\mathbf{r}-\mathbf{r}')$ and is related to the Green function for the electric field (defined in the previous paragraph), $\mathbf{G}(\mathbf{r},\mathbf{r}',\omega)$, by:

$$G_{ij}(\mathbf{r},\mathbf{r}',\omega) = -\frac{c^2}{\omega^2}\partial_i\partial'_j G^\phi(\mathbf{r},\mathbf{r}',\omega).$$

We can compute the Green function for an both an anisotropic and an isotropic polar crystal with the same methods. As is well known for a 2D-translationally-invariant system, the Green function can be expressed in terms of a Fourier integral over wavevectors. This Fourier integral (for the polaritons) in the region above the dielectric slab is known once one finds the p-polarized reflectivity of the system, r_p. One finds that for an isotropic slab of polar dielectric of thickness d and permittivity ϵ with a superstrate of air and a non-dispersive substrate of dielectric constant ϵ_s that:

$$r_p = \frac{e^{2qd}(\epsilon-1)(\epsilon_s+\epsilon) + (\epsilon+1)(\epsilon_s-\epsilon)}{e^{2qd}(\epsilon+1)(\epsilon_s+\epsilon) + (\epsilon-1)(\epsilon_s-\epsilon)}. \tag{8}$$

Similarly one finds that for an anisotropic slab of polar dielectric (like hBN) of thickness d and permittivity $\text{diag}(\epsilon_\perp, \epsilon_\perp, \epsilon_{||})$ with a superstrate of air and a non-dispersive substrate of dielectric constant ϵ_s that:

$$r_p = \frac{\left(\sqrt{r}\epsilon_{||}+i\right)\left(\epsilon_s + i\sqrt{r}\epsilon_{||}\right)e^{2iq\sqrt{r}d} + \left(\sqrt{r}\epsilon_{||}-i\right)\left(\epsilon_s - i\sqrt{r}\epsilon_{||}\right)}{\left(\sqrt{r}\epsilon_{||}-i\right)\left(\epsilon_s + i\sqrt{r}\epsilon_{||}\right)e^{2iq\sqrt{r}d} + \left(\sqrt{r}\epsilon_{||}+i\right)\left(\epsilon_s - i\sqrt{r}\epsilon_{||}\right)} \tag{9}$$

where r is the absolute value of the anisotropy ratio, defined by $r = \left|\frac{\epsilon_\perp}{\epsilon_{||}}\right|$. The location of the poles of the imaginary part of the reflectivity in (ω, q) space gives the dispersion relation $\omega(q)$. When losses are present, Im r_p is centered around the dispersion relation.

Macroscopic QED of SPhPs at First Order in Perturbation Theory

In [8], it was shown that the decay rate for a transition between states e and g (including the effects of material losses) is given by:

$$\Gamma = \frac{e^2}{2\hbar\epsilon_0 m_e^2 \omega_0^2} \frac{1}{(2\pi)^2} \int d\mathbf{q}\, q |\langle g| \hat{\boldsymbol{e}}^*(\mathbf{q}) e^{-i\mathbf{q}\cdot\boldsymbol{\rho}-qz} \cdot \mathbf{p} + \mathbf{p} \cdot \hat{\boldsymbol{e}}^*(\mathbf{q}) e^{-i\mathbf{q}\cdot\boldsymbol{\rho}-qz} |e\rangle|^2 \,\mathrm{Im}\, r_p,$$

where r_p is the p-polarized reflectivity of the air-polar dielectric-substrate system. There's a rather computationally simple way to evaluate the matrix element that is applicable for electronic systems with cylindrical symmetry, and for photonic modes which are highly confined and well-described by a scalar potential (which our modes of interest are). Suppose that $\hat{\boldsymbol{e}}^*(\mathbf{q}) e^{-i\mathbf{q}\cdot\boldsymbol{\rho}-qz} = \nabla\varphi$. In this case, $\varphi = \frac{i}{\sqrt{2}q} e^{-i\mathbf{q}\cdot\rho-qz}$. Then it follows that the matrix above can be expressed in terms of this scalar potential:

$$\left| \frac{e}{2m} \int d\mathbf{r}\, \psi_g^* \left(\mathbf{p} \cdot \nabla\varphi + \nabla\varphi \cdot \mathbf{p} \right) \psi_e \right| = \left| e\omega_{eg} \int d\mathbf{r}\, \varphi \psi_g^* \psi_e \right|. \tag{10}$$

This result can be easily derived by making use of integration by parts and the Schrodinger wave equation for the electron. Note that although we're representing the field by a scalar potential, we did not perform a change of gauge. We merely took advantage of a mathematical relation that applies for longitudinal (curl-free) fields. To proceed, we represent φ in terms of Bessel functions through the Jacobi-Anger expansion:

$$e^{i\mathbf{q}\cdot\boldsymbol{\rho}} = e^{iq\rho\cos(\alpha-\phi)} = \sum_{n=-\infty}^{\infty} i^n J_n(q\rho) e^{in(\alpha-\phi)}, \tag{11}$$

where α is the angle between $\mathbf{q}$ and an in-plane reference direction $\hat{x}$, ϕ is the angle between the electron position and this direction, and ρ is the in-plane radial position measured from the center of the atom. It follows that the decay rate, assuming that the final state has z-projected angular momentum m_g and the initial state has z-projected angular momentum m_e (this is where cylindrical symmetry comes in), and defining $\Delta m = m_g - m_e$ is:

$$\Gamma = 2\alpha c \int dq\, |\langle g| J_{\Delta m}(q\rho) e^{-i\Delta m\phi} e^{-qz} |e\rangle|^2 \,\mathrm{Im}\, r_p. \tag{12}$$

For a pure multipolar emitter of order n, where $n = 1$ for dipole, $n = 2$ for quadrupole, etc., the matrix element scales like q^{2n}, as we verified numerically and as is consistent with what was found in [8].

Macroscopic QED at Higher Order in Perturbation Theory: Emission of Two Polaritons

In this section, we derive the frequency spectra of spontaneous emission of two excitations of the lossy electromagnetic field. These results incorporate losses and thus elucidate the contribution of quenching and polariton launching to the decay of an excited emitter. The derivation proceeds by application of the Fermi Golden rule at second order in perturbation theory as applied to transitions between an initial state $|e,0\rangle$ and a continuum of final states with two excitations of the lossy electromagnetic field, i.e., $|g,\mathbf{x}\omega k,\mathbf{x}'\omega' k'\rangle$. Fermi's Golden Rule for this decay reads:

$$\Gamma=\frac{2\pi}{\hbar^2}\frac{1}{2}\int d\mathbf{r}d\mathbf{r}'\int d\omega d\omega'\sum_{k,k'}\Big|\sum_{i_1}\frac{\langle g,\mathbf{r}\omega k,\mathbf{r}'\omega' k'|V|i_1\rangle\langle i_1|V|e,0\rangle}{E_e-E_{i_1}+i0^+}\Big|^2\delta(\omega_0-\omega-\omega'), \quad (13)$$

where $|i_1\rangle$ are intermediate states containing both the atom and field degrees of freedom. The sum is understood to be a sum over discrete degrees of freedom and an integral over continuous ones. The factor of $1/2$ comes from the fact that when we sum over all $\{\mathbf{r}\omega k,\mathbf{r}'\omega' k\}$ pairs, each pair of excitations appears twice. To proceed, we express the field operators in terms of Green functions and use three facts:

1.

$$\begin{aligned}V_{i_j,i_{j-1}}&=\langle n_j,\mathbf{x}_j\omega_j k_j,\mathbf{x}_{j-1}\omega_{j-1}k_{j-1},..,.\mathbf{x}_1\omega_1 k_1|d_iE_i|n_{j-1},\mathbf{x}_{j-1}\omega_{j-1}k_{j-1},...,\mathbf{x}_1\omega_1 k_1\rangle\\&=i\sqrt{\frac{\hbar}{\pi\epsilon_0}}d_{i_j}^{n_j,n_{j-1}}\frac{\omega_j^2}{c^2}\sqrt{\text{Im }\epsilon(\mathbf{x}_j,\omega_j)}G^*_{i_j,k_j}(\mathbf{r}_0,\mathbf{x}_j,\omega_j),\end{aligned} \quad (14)$$

2.

$$\frac{\omega^2}{c^2}\int d\mathbf{r}\ \text{Im }\epsilon(\mathbf{r},\omega)(GG^\dagger)(\mathbf{r}_0,\mathbf{r},\omega)=\text{Im }G(\mathbf{r}_0,\mathbf{r}_0,\omega),\text{ and}$$

3. For a photonic medium which is translationally invariant in-plane (as is the system we consider throughout the text):

$$\text{Im }G_{ij}(\mathbf{r}_0,\mathbf{r}_0,\omega)=\frac{\omega}{6\pi c}F_p(\mathbf{r}_0,\mathbf{r}_0,\omega)D_{ij},$$

where $D=\text{diag}(1/2,1/2,1)$ and F_p is the Purcell factor for one-photon emission for the z-polarized dipole (frequency ω and position $\mathbf{r}_0$) near this material [49]. As a reminder, this Purcell factor is equal to $\frac{3c^3}{2\omega^3}\int dq\ q^2e^{-2qz_0}\text{Im }r_p(q,\omega)$.

Defining (note that this definition differs from that in the main text by a factor of the squared electron charge)

$$T_{ij}(\omega)=\sum_n\frac{x_j^{gn}x_i^{ne}}{\omega_e-\omega_n-\omega}+\frac{x_i^{gn}x_j^{ne}}{\omega_e-\omega_n-(\omega_0-\omega)}=T_{ji}(\omega_0-\omega),$$

we see that the second-order emission spectrum becomes:

$$\frac{d\Gamma}{d\omega} = \frac{4\alpha^2}{9\pi c^4}\,\omega^3(\omega_0-\omega)^3 F_p(\omega)F_p(\omega_0-\omega)\sum_{i,j,r,s} D_{ri}D_{sj}T_{ij}(\omega)T_{rs}(\omega)^*, \tag{15}$$

Because D is diagonal, this is simply:

$$\frac{d\Gamma}{d\omega} = \frac{4\alpha^2}{9\pi c^4}\omega^3(\omega_0-\omega)^3 F_p(\omega)F_p(\omega_0-\omega)\sum_{ij} D_{ii}D_{jj}|T_{ij}|^2. \tag{16}$$

We focus on the case in which the transition is between two s states. In that case, only the diagonal terms of T_{ij} are relevant meaning that the above sum over i,j becomes $\frac{3}{2}T_{zz}$, making the differential emission rate for two lossy excitations:

$$\frac{d\Gamma}{d\omega} = \frac{2}{3\pi c^4}\alpha^2\omega^3(\omega_0-\omega)^3 F_p(\omega)F_p(\omega_0-\omega)|T_{zz}|^2 \tag{17}$$

Using the fact that the free-space differential decay rate is given by [50]:

$$\frac{4}{3\pi c^4}\alpha^2\omega^3(\omega_0-\omega)^3|T_{zz}|^2,$$

it follows that the spectral enhancement (defined in the main text) is:

$$\frac{\frac{d\Gamma}{d\omega}}{\frac{d\Gamma_0}{d\omega}} = \frac{1}{2}F_p(\omega)F_p(\omega_0-\omega). \tag{18}$$

By evaluating the T_{ij} tensors, we can easily go from the spectral enhancement factors to the two-photon Purcell factor by evaluating the sum over states, as we do in order to get the rates claimed in the main text. Moreover, the actual decay rate can easily be estimated in the case where the bandwidth of the polaritons is narrow (as is the case in what we consider) as:

$$\Gamma \approx \frac{\alpha^2}{96\pi c^4}\omega_0^6\left|T_{zz}\left(\frac{\omega_0}{2}\right)\right|^2\int d\omega\; F_p(\omega)F_p(\omega_0-\omega), \tag{19}$$

in the case where the emission spectrum is sharply centered at $\frac{\omega_0}{2}$ as a result of the sharpness of the spectral enhancement.

We conclude this section by showing calculated results (Figure 5) for the spectral enhancement of two-photon $s \rightarrow s$ transitions for an emitter in the vicinity of hexagonal boron nitride. Its consequences are discussed in the main text.

Lossless Limit: Effective Mode Expansion

This section develops a mode expansion formalism, comparing it to the Green function formalism used so far, and discusses their relative strengths and weaknesses. Although all of the

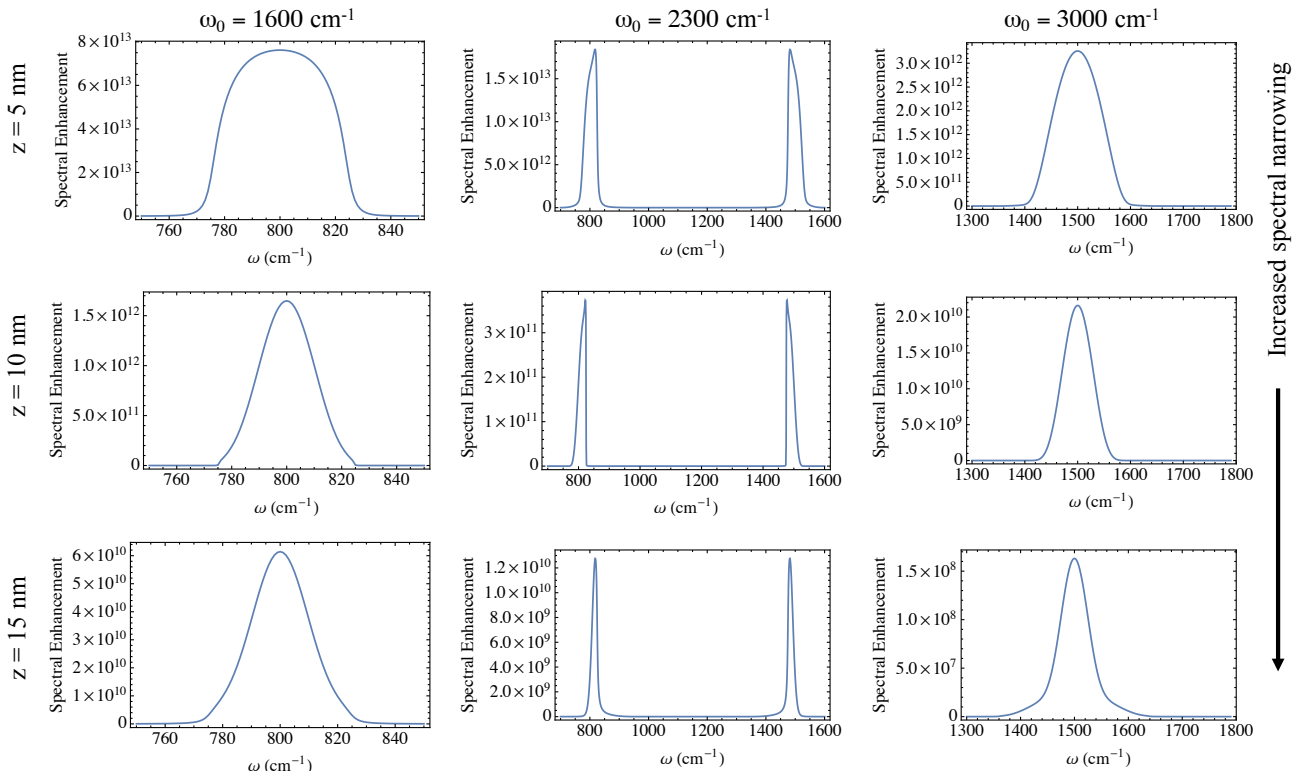

FIG. 5: **General Features of Two-Polariton Emission: Purcell Spectra.** Two-polariton Purcell spectra defined as in Equation (4) for a spherical emitter as a function of emitter frequency (1600 (left), 2300 (center), and 3000 (right) cm^{-1}) and emitter separation (5 (top), 10 (center), and 15 (bottom) nm). Hyperbolicity allows for enhancement over a large range of frequencies compared to isotropic systems. Moreover, distance can be used to tune the width of the spectrum.

decay rates that we compute can be computed through the Green function formalism presented in the previous section, it is difficult to extract information such as the angular spectrum of emitted polaritons from this formalism (which we define as the angular spectrum in the lossless limit). The reason for this difficulty is that concepts like the angular spectrum are clearly most naturally computed when one assumes that the excitations coupled to are modes labeled by their direction of propagation. Therefore, to compute the angular spectrum of emitted radiation, we use a formalism different from the one used in the previous sections. We will write down field operators appropriate to the lossless situation and compute the spectrum of two-polariton emission by using Fermi's Golden Rule with these field operators.

It is known that in lossless and non-dispersive dielectrics, the vector potential can be expressed

in the form of a mode expansion:

$$\mathbf{A} = \sum_n \sqrt{\frac{\hbar}{2\epsilon_0 \omega_n}} \left(\mathbf{F}_n a_n + hc\right),$$

where the $\mathbf{F}_n$ are the orthonormal modes of the Maxwell equations, normalized suitably. In [46], it was rigorously shown by taking the Green function formalism in the lossless limit that a mode expansion for the field operators in terms of eigenmodes (of the form above) can be derived for polaritons. In this effective mode expansion, the field modes are normalized such that:

$$\frac{\epsilon_0}{2\omega} \int d\mathbf{r}\, \mathbf{F}^*(\mathbf{r}) \cdot \frac{d(\epsilon_r \omega^2)}{d\omega} \cdot \mathbf{F}(\mathbf{r}) = \frac{\hbar\omega}{2}.$$

We take as the normalization or quantization volume one which is infinite in the z-direction and has area 1 m^2 in the in-plane direction. In the electrostatic limit $\frac{qc}{\omega} \gg 1$, the fields in the vicinity of a well-localized emitter above a polar dielectric are of the form

$$\mathbf{F} \sim e^{i\mathbf{q}\cdot\boldsymbol{\rho} - qz} \hat{e}(\hat{\mathbf{q}}), \tag{20}$$

where $\hat{e}(\hat{\mathbf{q}}) \equiv \frac{\hat{\mathbf{q}} + i\hat{\mathbf{z}}}{\sqrt{2}}$. $\hat{\mathbf{q}}$ can be expressed as $\cos\theta\hat{\mathbf{x}} + \sin\theta\hat{\mathbf{y}}$. We use this fact to compute the angular spectrum of pairs of emitted phonon-polaritons in what follows.

We conclude this part of the discussion by noting that effective mode expansion was shown by proving that the denominator of the Fourier transformed Green function in the lossless limit is proportional to the energy term in the previous equation. Although we derived this result on very general grounds (see [46]), we explicitly show the equivalence here as a consistency check on our calculations. In Figure 6, we compare predictions of the mode-expansion formalism and the Green function formalism taken in the zero loss limit. The particular prediction we address is the Purcell factor of a z-polarized dipole some distance away from hexagonal boron nitride ((a) and (b)) or cubic boron nitride (c). As can be seen, aside from small numerical integration error, these predictions match extremely well. In Figure 7, we consider the same Purcell factor but now we compare the lossless value of the Purcell factor to the Purcell factor when realistic losses are incorporated into the Lorentz permittivities of hexagonal boron nitride and cubic boron nitride ($\gamma = 5$ cm^{-1} is taken in all three cases). We can see that these predictions agree reasonably well.

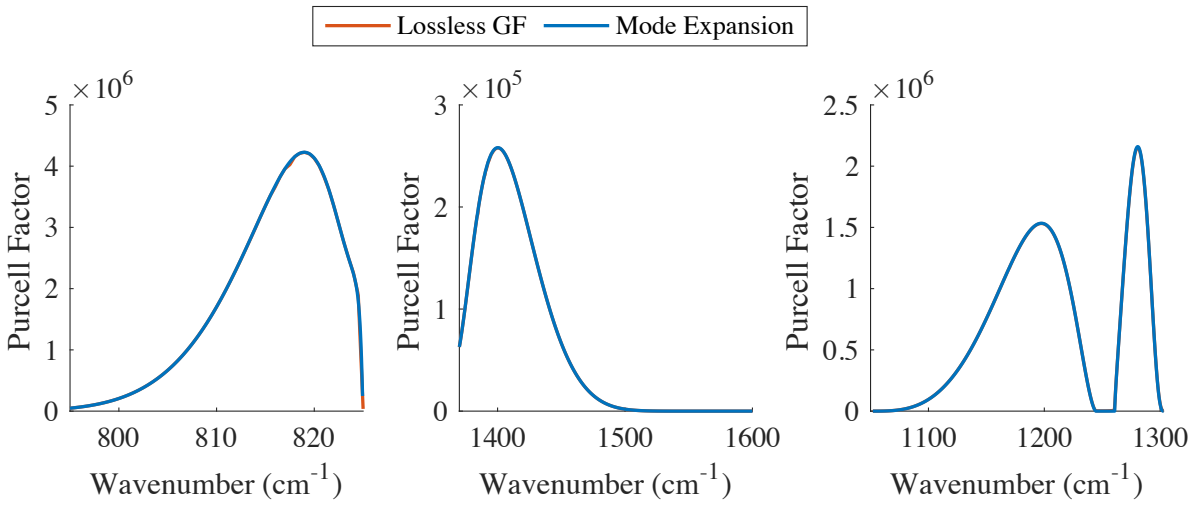

FIG. 6: **Comparison of Lossless Green Function Formalism and Mode Expansion** Purcell Factors calculated for (a) the lower Reststrahlen band of hBN for an hBN thickness of 2 nm and emitter-surface separation of 10 nm (b) the upper Reststrahlen band of hBN for an hBN thickness of 2 nm and emitter-surface separation of 10 nm (c) the Reststrahlen band of cBN for a cBN thickness of 5 nm and emitter-surface separation of 10 nm.

Angular Spectrum of Emitted Phonon Polaritons

Now, we focus on computing the angular spectrum of radiation of phonon-polaritons emitted by an excited atomic electron. In other words, we want the quantity

$$S(\omega,\theta,\theta') \equiv \frac{d\Gamma}{d\omega d\theta d\theta'}.$$

Because we want to focus only on excitation of propagating polaritons and not loss-excitations, we extract the pole contribution from the imaginary part of the p-polarized reflectivity. This is equivalent to writing field operators in the lossless limit. Writing the second-order Fermi Golden Rule for the transition rate between an initial state $|e,0\rangle$ and the continuum of final states $|g,\mathbf{q}\mathbf{q}'\rangle$, we see that:

$$\frac{d\Gamma}{d\omega d\theta d\theta'} = \frac{1}{16\pi^3\hbar^2}\frac{q(\omega)q(\omega_0-\omega)}{v_g(\omega)v_g(\omega_0-\omega)}\left|\sum_{i_1}\frac{\langle g,\mathbf{q}\mathbf{q}'|\mathbf{d}\cdot\mathbf{E}|i_1\rangle\langle i_1|\mathbf{d}\cdot\mathbf{E}|e,0\rangle}{E_e-E_{i_1}+i0^+}\right|^2,$$

where v_g is the group velocity, $\frac{d\omega}{dq}$. Inserting the definition of the operators, we find that the spectrum is given by:

$$S(\omega,\theta,\theta') = \frac{\alpha^2c^2}{4\pi}\omega(\omega_0-\omega)\frac{q(\omega)q(\omega_0-\omega)}{v_g(\omega)v_g(\omega_0-\omega)}\left|F^{*i}_{\mathbf{q}}F^{*j}_{\mathbf{q}'}T_{ij}\right|^2 \tag{21}$$

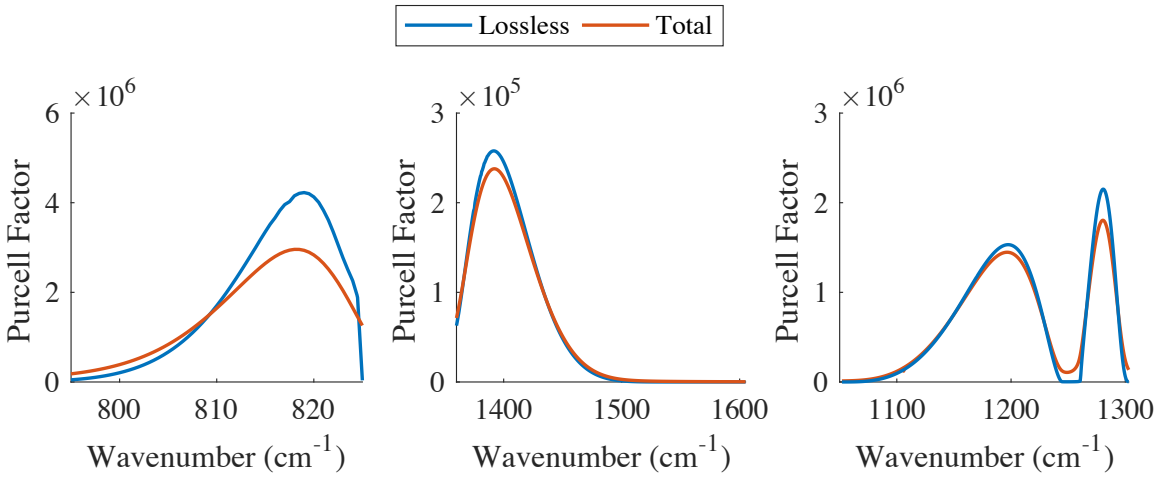

FIG. 7: **Comparison of Green Function Formalism with Losses and Mode Expansion** Purcell Factors calculated for (a) the lower Reststrahlen band of hBN for an hBN thickness of 2 nm and emitter-surface separation of 10 nm (b) the upper Reststrahlen band of hBN for an hBN thickness of 2 nm and emitter-surface separation of 10 nm (c) the Reststrahlen band of cBN for a cBN thickness of 5 nm and emitter-surface separation of 10 nm.

where

$$T_{ij}(\omega) = \sum_n \frac{x_j^{gn} x_i^{ne}}{\omega_i - \omega_n - \omega} + \frac{x_i^{gn} x_j^{ne}}{\omega_i - \omega_n - (\omega_0 - \omega)} = T_{ji}(\omega_0 - \omega).$$

We now use this to extract the form of the angular spectrum of entangled photons as a function of the electronic orbitals participating in the transition. To give the reader a sense of how much control one may have over the angular spectrum of emitted photon pairs, we consider four cases. In all four, the final states are s states. But the initial states will be taken to be s, d_{xy}, d_{yz}, and d_{xz} states.

$s \to s$

In the case where the initial state is an s state, we have that $T_{ij} = 0$ if $i \neq j$. This is because of the dipole approximation, which fixes the intermediate state to be a p state. Therefore, if $i \neq j$, then T_{ij} has a sum of terms like $\langle s|x_i|p_k\rangle\langle p_k|x_j|s\rangle$, where $p_k = p_x, p_y, p_z$. Each of these terms individually vanishes, and so the entire tensor vanishes. Moreover $T_{xx} = T_{yy} = T_{zz} \equiv T$ because

$\langle p_x|x|s\rangle = \langle p_y|y|s\rangle = \langle p_z|z|s\rangle$: Therefore:

$$S(\omega,\theta,\theta') = |T|^2\left(\cos\theta\cos\theta' + \sin\theta\sin\theta' - 1\right)^2 = 4|T|^2\sin^4\left(\frac{\theta-\theta'}{2}\right). \ (s \to s) \tag{22}$$

$d_{xy} \to s$

In the case where the initial state is d_{xy}, the only contributing terms are T_{xy} and T_{yx}. The argument for this statement makes use of the fact that the d_{xy} has an angular dependence that can be written in Cartesian coordinates as xy. We start proving this claim by examing the T_{zi} components. If one of the indices is z, then it will either be the case that the intermediate state must be a p_z state (to have overlap with the s state), or that there will be a matrix element of the form $\langle p_i|z|d_{xy}\rangle$. The first case gives zero because d_{xy} has no transition dipole moment with z. The second case also gives zero because d_{xy} has no z-polarized dipole moment with any p orbital. Thus the T_{zi} components vanish. The T_{xx} and T_{yy} components also vanish because d_{xy} has no (x,y)-polarized dipole moment with $p_{x,y}$. Therefore:

$$S(\omega,\theta,\theta') = \left(T_{xy}(\omega)\cos\theta\sin\theta' + T_{xy}(\omega_0-\omega)\sin\theta\cos\theta'\right)^2. \ (d_{xy} \to s) \tag{23}$$

$d_{xz} \to s$ and $d_{yz} \to s$

A nearly identical argument to the one above (replace all y's with z's or all x's with z's) yields:

$$S(\omega,\theta,\theta') = \left(T_{xz}(\omega)\cos\theta + T_{xz}(\omega_0-\omega)\cos\theta'\right)^2. \ (d_{xz} \to s) \tag{24}$$

$$S(\omega,\theta,\theta') = \left(T_{yz}(\omega)\sin\theta + T_{yz}(\omega_0-\omega)\sin\theta'\right)^2. \ (d_{yz} \to s) \tag{25}$$

---

[1] Harry A Atwater. The promise of plasmonics. *Scientific American*, 296(4):56–62, 2007.

[2] Martin Moskovits. Surface-enhanced spectroscopy. *Reviews of modern physics*, 57(3):783, 1985.

[3] Martin Moskovits. Surface-enhanced raman spectroscopy: a brief retrospective. *Journal of Raman Spectroscopy*, 36(6-7):485–496, 2005.

[4] Martti Kauranen and Anatoly V Zayats. Nonlinear plasmonics. *Nature Photonics*, 6(11):737–748, 2012.

[5] Hans A Bethe and Edwin E Salpeter. *Quantum mechanics of one-and two-electron atoms*. Springer Science & Business Media, 2012.

[6] A Rubinowicz. Multipole radiation in atomic spectra. *Reports on progress in physics*, 12(1):233, 1949.

[7] Edward Uhler Condon and George Hiram Shortley. *The theory of atomic spectra*. Cambridge University Press, 1951.

[8] Nicholas Rivera, Ido Kaminer, Bo Zhen, John D Joannopoulos, and Marin Soljačić. Shrinking light to allow forbidden transitions on the atomic scale. *Science*, 353(6296):263–269, 2016.

[9] Matthew Pelton. Modified spontaneous emission in nanophotonic structures. *Nature Photonics*, 9(7):427–435, 2015.

[10] Alex Hayat, Pavel Ginzburg, and Meir Orenstein. Measurement and model of the infrared two-photon emission spectrum of gaas. *Physical review letters*, 103(2):023601, 2009.

[11] Yasutomo Ota, Satoshi Iwamoto, Naoto Kumagai, and Yasuhiko Arakawa. Spontaneous two-photon emission from a single quantum dot. *Physical review letters*, 107(23):233602, 2011.

[12] Amir Nevet, Nikolai Berkovitch, Alex Hayat, Pavel Ginzburg, Shai Ginzach, Ofir Sorias, and Meir Orenstein. Plasmonic nanoantennas for broad-band enhancement of two-photon emission from semiconductors. *Nano letters*, 10(5):1848–1852, 2010.

[13] Alex Hayat, Pavel Ginzburg, and Meir Orenstein. Observation of two-photon emission from semiconductors. *Nature photonics*, 2(4):238–241, 2008.

[14] Vladimir Borisovich Berestetskii, Evgenii Mikhailovich Lifshitz, and Lev Petrovich Pitaevskii. *Quantum electrodynamics*, volume 4. Butterworth-Heinemann, 1982.

[15] Zhe Fei, Gregory O Andreev, Wenzhong Bao, Lingfeng M Zhang, Alexander S. McLeod, Chen Wang, Margaret K Stewart, Zeng Zhao, Gerardo Dominguez, Mark Thiemens, et al. Infrared nanoscopy of dirac plasmons at the graphene–sio2 interface. *Nano letters*, 11(11):4701–4705, 2011.

[16] Tony Low and Phaedon Avouris. Graphene plasmonics for terahertz to mid-infrared applications. *Acs Nano*, 8(2):1086–1101, 2014.

[17] Hugen Yan, Tony Low, Wenjuan Zhu, Yanqing Wu, Marcus Freitag, Xuesong Li, Francisco Guinea, Phaedon Avouris, and Fengnian Xia. Damping pathways of mid-infrared plasmons in graphene nanostructures. *Nature Photonics*, 7(5):394–399, 2013.

[18] Marinko Jablan, Hrvoje Buljan, and Marin Soljačić. Plasmonics in graphene at infrared frequencies. *Physical review B*, 80(24):245435, 2009.

[19] Frank HL Koppens, Darrick E Chang, and F Javier Garcia de Abajo. Graphene plasmonics: a platform for strong light–matter interactions. *Nano letters*, 11(8):3370–3377, 2011.

[20] Qiming Zhang, Xiangping Li, Md Muntasir Hossain, Yunzhou Xue, Jie Zhang, Jingchao Song, Jingying Liu, Mark D Turner, Shanhui Fan, Qiaoliang Bao, et al. Graphene surface plasmons at the near-infrared optical regime. *Scientific reports*, 4, 2014.

[21] Achim Woessner, Mark B Lundeberg, Yuanda Gao, Alessandro Principi, Pablo Alonso-González, Matteo Carrega, Kenji Watanabe, Takashi Taniguchi, Giovanni Vignale, Marco Polini, et al. Highly confined low-loss plasmons in graphene–boron nitride heterostructures. *Nature materials*, 2014.

[22] AN Grigorenko, Marco Polini, and KS Novoselov. Graphene plasmonics. *Nature photonics*, 6(11):749–758, 2012.

[23] Tadaaki Nagao, Torsten Hildebrandt, Martin Henzler, and Shuji Hasegawa. Dispersion and damping of a two-dimensional plasmon in a metallic surface-state band. *Physical review letters*, 86(25):5747, 2001.

[24] Sung Jin Park and Richard E. Palmer. Acoustic plasmon on the au(111) surface. *Phys. Rev. Lett.*, 105:016801, 2010.

[25] Bogdan Diaconescu, Karsten Pohl, Luca Vattuone, Letizia Savio, Philip Hofmann, Vyacheslav M Silkin, Jose M Pitarke, Eugene V Chulkov, Pedro M Echenique, Daniel Farías, et al. Low-energy acoustic plasmons at metal surfaces. *Nature*, 448(7149):57–59, 2007.

[26] EP Rugeramigabo, T Nagao, and H Pfnür. Experimental investigation of two-dimensional plasmons in a dysi 2 monolayer on si (111). *Physical Review B*, 78(15):155402, 2008.

[27] KJ Tielrooij, L Orona, A Ferrier, M Badioli, G Navickaite, S Coop, S Nanot, B Kalinic, T Cesca, L Gaudreau, et al. Electrical control of optical emitter relaxation pathways enabled by graphene. *Nature Physics*, 2015.

[28] Zhe Fei, AS Rodin, GO Andreev, W Bao, AS McLeod, M Wagner, LM Zhang, Z Zhao, M Thiemens, G Dominguez, et al. Gate-tuning of graphene plasmons revealed by infrared nano-imaging. *Nature*, 487(7405):82–85, 2012.

[29] C Sánchez Muñoz, E Del Valle, A González Tudela, K Müller, S Lichtmannecker, M Kaniber, C Tejedor, JJ Finley, and FP Laussy. Emitters of n-photon bundles. *Nature photonics*, 8(7):550–555, 2014.

[30] R Hillenbrand, T Taubner, and F Keilmann. Phonon-enhanced light–matter interaction at the nanometre scale. *Nature*, 418(6894):159–162, 2002.

[31] S Dai, Z Fei, Q Ma, AS Rodin, M Wagner, AS McLeod, MK Liu, W Gannett, W Regan, K Watanabe,

et al. Tunable phonon polaritons in atomically thin van der waals crystals of boron nitride. *Science*, 343(6175):1125–1129, 2014.

[32] Xiaoji G Xu, Jian-Hua Jiang, Leonid Gilburd, Rachel G Rensing, Kenneth S Burch, Chunyi Zhi, Yoshio Bando, Dmitri Golberg, and Gilbert C Walker. Mid-infrared polaritonic coupling between boron nitride nanotubes and graphene. *ACS nano*, 8(11):11305–11312, 2014.

[33] S Dai, Q Ma, MK Liu, T Andersen, Z Fei, MD Goldflam, M Wagner, K Watanabe, T Taniguchi, M Thiemens, et al. Graphene on hexagonal boron nitride as a tunable hyperbolic metamaterial. *Nature nanotechnology*, 10(8):682–686, 2015.

[34] S Dai, Q Ma, T Andersen, AS Mcleod, Z Fei, MK Liu, M Wagner, K Watanabe, T Taniguchi, M Thiemens, et al. Subdiffractional focusing and guiding of polaritonic rays in a natural hyperbolic material. *Nature communications*, 6, 2015.

[35] Peining Li, Martin Lewin, Andrey V Kretinin, Joshua D Caldwell, Kostya S Novoselov, Takashi Taniguchi, Kenji Watanabe, Fabian Gaussmann, and Thomas Taubner. Hyperbolic phonon-polaritons in boron nitride for near-field optical imaging and focusing. *Nature communications*, 6, 2015.

[36] Kaijun Feng, William Streyer, SM Islam, Jai Verma, Debdeep Jena, Daniel Wasserman, and Anthony J Hoffman. Localized surface phonon polariton resonances in polar gallium nitride. *Applied Physics Letters*, 107(8):081108, 2015.

[37] Andrea Tomadin, Alessandro Principi, Justin CW Song, Leonid S Levitov, and Marco Polini. Accessing phonon polaritons in hyperbolic crystals by angle-resolved photoemission spectroscopy. *Physical review letters*, 115(8):087401, 2015.

[38] Edward Yoxall, Martin Schnell, Alexey Y Nikitin, Oihana Txoperena, Achim Woessner, Mark B Lundeberg, Félix Casanova, Luis E Hueso, Frank HL Koppens, and Rainer Hillenbrand. Direct observation of ultraslow hyperbolic polariton propagation with negative phase velocity. *Nature Photonics*, 2015.

[39] Joshua D Caldwell and Kostya S Novoselov. Van der waals heterostructures: Mid-infrared nanophotonics. *Nature materials*, 14(4):364–366, 2015.

[40] Joshua D Caldwell, Andrey V Kretinin, Yiguo Chen, Vincenzo Giannini, Michael M Fogler, Yan Francescato, Chase T Ellis, Joseph G Tischler, Colin R Woods, Alexander J Giles, et al. Subdiffractional volume-confined polaritons in the natural hyperbolic material hexagonal boron nitride. *Nature communications*, 5, 2014.

[41] Joshua D Caldwell, Orest J Glembocki, Yan Francescato, Nicholas Sharac, Vincenzo Giannini, Fran-

cisco J Bezares, James P Long, Jeffrey C Owrutsky, Igor Vurgaftman, Joseph G Tischler, et al. Low-loss, extreme subdiffraction photon confinement via silicon carbide localized surface phonon polariton resonators. *Nano letters*, 13(8):3690–3697, 2013.

[42] Joshua D Caldwell, Lucas Lindsay, Vincenzo Giannini, Igor Vurgaftman, Thomas L Reinecke, Stefan A Maier, and Orest J Glembocki. Low-loss, infrared and terahertz nanophotonics using surface phonon polaritons. *Nanophotonics*, 4(1), 2015.

[43] Jacob B Khurgin. How to deal with the loss in plasmonics and metamaterials. *Nature nanotechnology*, 10(1):2–6, 2015.

[44] MS Tame, KR McEnery, ŞK Özdemir, J Lee, SA Maier, and MS Kim. Quantum plasmonics. *Nature Physics*, 9(6):329–340, 2013.

[45] Ludwig Knöll, Stefan Scheel, and Dirk-Gunnar Welsch. Qed in dispersing and absorbing media. Technical report, 2000.

[46] Xiao Lin, Nicholas Rivera, Josué J López, Ido Kaminer, Hongsheng Chen, and Marin Soljačić. Tailoring the energy distribution and loss of 2d plasmons. *arXiv preprint arXiv:1609.01794*, 2016.

[47] Anshuman Kumar, Tony Low, Kin Hung Fung, Phaedon Avouris, and Nicholas X Fang. Tunable light–matter interaction and the role of hyperbolicity in graphene–hbn system. *Nano letters*, 15(5):3172–3180, 2015.

[48] Claude Cohen-Tannoudji, Jacques Dupont-Roc, Gilbert Grynberg, and Patricia Thickstun. *Atom-photon interactions: basic processes and applications*. Wiley Online Library, 1992.

[49] A Femius Koenderink. On the use of purcell factors for plasmon antennas. *Optics letters*, 35(24):4208–4210, 2010.

[50] G Breit and E Teller. Metastability of hydrogen and helium levels. *The Astrophysical Journal*, 91:215, 1940.

[51] It is important to note though that if the bandwidth of the highly confined modes is too small, then the phase space for emission becomes too small and the rates are correspondingly slow. This makes very high-Q optical cavities not well suited for the effects that we describe here